Journal of Power Sources 215 (2012) 53–62

Contents lists available at SciVerse ScienceDirect

Journal of Power Sources

journal homepage: www.elsevier.com/locate/jpowsour

An optimization study of PtSn/C catalysts applied to direct ethanol fuel cell: Effect of the preparation method on the electrocatalytic activity of the catalysts

T.S. Almeida [a], L.M. Palma [a], P.H. Leonello [a], C. Morais [b], K.B. Kokoh [b], A.R. De Andrade [a,*]

[a] Departamento de Química, Faculdade de Filosofia Ciências e Letras de Ribeirão Preto, Universidade de São Paulo, 14040-901 Ribeirão Preto, SP, Brasil
[b] Université de Poitiers, IC2MP UMR CNRS 7285, "Equipe E-lyse", 4 rue Michel Brunet B27, BP 633, 86022 Poitiers Cedex, France

HIGHLIGHTS

- We have optimized the preparation of PtSn/C catalysts by the microwave-assisted method.
- The microwave-assisted heating promotes nanoelectrocatalysts with high current density.
- This method requires short preparation time, which is advantageous compared to other methods proposed in the literature.
- Propylene glycol and sodium acetate produces nanocatalysts with ranging from 2.0 to 5.0 nm and high catalytic activity

ARTICLE INFO

Article history:
Received 14 March 2012
Received in revised form
19 April 2012
Accepted 20 April 2012
Available online 8 May 2012

Keywords:
PtSn nanoparticles
Ethanol oxidation
Microwave-assisted method
Thermal decomposition of polymeric precursors
Electrocatalysis

ABSTRACT

The aim of this work was to perform a systematic study of the parameters that can influence the composition, morphology, and catalytic activity of PtSn/C nanoparticles and compare two different methods of nanocatalyst preparation, namely microwave-assisted heating (MW) and thermal decomposition of polymeric precursors (DPP). An investigation of the effects of the reducing and stabilizing agents on the catalytic activity and morphology of $Pt_{75}Sn_{25}$/C catalysts prepared by microwave-assisted heating was undertaken for optimization purposes. The effect of short-chain alcohols such as ethanol, ethylene glycol, and propylene glycol as reducing agents was evaluated, and the use of sodium acetate and citric acid as stabilizing agents for the MW procedure was examined. Catalysts obtained from propylene glycol displayed higher catalytic activity compared with catalysts prepared in ethylene glycol. Introduction of sodium acetate enhanced the catalytic activity, but this beneficial effect was observed until a critical acetate concentration was reached. Optimization of the MW synthesis allowed for the preparation of highly dispersed catalysts with average sizes lying between 2.0 and 5.0 nm. Comparison of the best catalyst prepared by MW with a catalyst of similar composition prepared by the polymeric precursors method showed that the catalytic activity of the material can be improved when a proper condition for catalyst preparation is achieved.

1. Introduction

Direct Alcohol Fuel Cells (DAFCs) have become increasingly attractive as an energy source for use in various portable devices. However, one of the major drawbacks to their implementation is the high catalyst cost. Utilization of electrode materials with high catalytic activity is required for operation at low temperatures (50–90 °C), so as to compensate for the low efficiency of the kinetic process. This means that precious metals like Pt and Pd should be employed [1–5]. However, pure metals alone do not provide satisfactory catalytic efficiency, due to rapid poisoning of the catalytic sites by impurities present in the fuels and/or by intermediates generated during the oxidation reaction. To overcome this problem, other metals are frequently associated with Pt and Pd. This give rise to plurimetallic alloys that confer the desired high efficiency to electrocatalytic materials [6–11].

Researchers have searched not only for catalysts with different chemical compositions but also for novel preparation routes. The use of different methodologies for the synthesis of metal nanoparticles supported on high surface area carbon or other conducting supports plays a crucial role in the development of fuel cell technology [9,11,12]. Many research groups have described that the activity of these materials is highly dependent on their composition, morphology, and size [13,14]. Thus, several methods for the

* Corresponding author.
E-mail address: ardandra@ffclrp.usp.br (A.R. De Andrade).

0378-7753
doi:10.1016/j.jpowsour.2012.04.061

synthesis of nanostructured catalysts have been developed, aiming to obtain materials with homogeneous metallic distribution, small particle size, and high catalytic activity [11,15–17].

Table 1 lists particle sizes for various PtSn/C compositions prepared by some of the methods normally employed in the literature.

The use of a reducing agent such as sodium borohydride is convenient. In combination with other strategies, this approach enables good control of nanoparticle size and composition. Dong-Ha Lim et al. [11] have used this methodology to synthesize PtSn/C catalysts with particle sizes ranging from 1.0 to 4.0 nm, and catalytic activity for ethanol oxidation of 14–56 mA mg_{Pt}^{-1} at 0.6 V *vs.* NHE. Godoy et al. [18] have prepared PtSn/C catalysts by the microemulsion method. These authors claimed that the reduction of metals trapped in the micelles allowed for good particle distribution and particle sizes around 2.5 nm was obtained. However, their catalytic activity for ethanol electrooxidation was less than 0.5 mA cm^{-2}.

Toshima and Yonezawa [29] have developed the alcohol reduction method, also known as the polyol method, with a view to obtaining colloidal nanoparticles dispersions with uniform particle size and homogeneous distribution. In this method, the reflux of an alcohol solution, usually ethylene glycol, containing the metallic ion and a stabilizing agent, normally a polymer, provides homogeneous colloidal dispersions of the corresponding metal nanoparticles. The alcohol simultaneously acts as solvent and reducing agent [16]. This method offers some advantages such as good reproducibility, satisfactory distribution, and small particle size. Moreover, it can be easily modified by addition of other reagents such as steric or electrostatic stabilizers, thus enabling better control of nanoparticle size and distribution on the carbon support.

Neto et al. [3] have investigated a series of PtRu/C, PtSn/C, and PtSnRu/C catalysts prepared by the alcohol reduction method using an ethylene glycol/water solution. Particle sizes in the order of 2.7 nm were achieved for the PtSn/C composition, which displayed catalytic activity close to 8.0 A g_{Pt}^{-1}. Spinacé et al. [20] have used the same method for the production of PtSn/C, PtRh, and PtSnRh/C catalysts. Their results were similar to those described by Neto et al. [3] i.e., small particle size (2.0 nm) was achieved, and particles were uniformly distributed on the carbon support, which culminated in significant catalytic activity for ethanol electrooxidation.

Dispersed platinum-based catalysts supported on carbon (Pt/C) for PEMFC fuel cells have been obtained by formic acid reduction [22,30]. In this methodology, catalysts are formed by addition of high surface area carbon support (Vulcan XC-72, Cabot) to a formic acid solution, used as reducing agent. The resulting mixture is heated to 80 °C, followed by addition of aliquots of a solution containing platinum and other metal salts to the reaction vessel. After complete metal reduction, the nanocatalyst is filtered, dried, and grounded. $Pt_{75}Sn_{25}$/C catalysts with particles sizes of 4.5 nm and experimental compositions close to the nominal ones have been prepared by the formic acid method [16]. However, these particles used as anode catalysts led to low power density i.e. 20 mW cm^{-2} for ethanol oxidation. Antolini et al. [22] have studied how ruthenium addition affects PtSn/C catalysts. Again, the desired catalytic composition and small particles (3.5 nm) homogeneously distributed onto the carbon support were obtained, but the power density was relatively low (28 mW cm^{-2}) for direct alcohol fuel cell.

The Thermal Decomposition of Polymeric Precursors (DPP), which is based on the Pechini method [31], has been extensively investigated by our group [23–25,27]. This method was initially developed for the preparation of thin films and was later adapted for preparation of materials in the powder form. It consists in dissolving metal salts in the presence of a hydroxyl acid (citric acid) and a polyhydroxylic alcohol (ethylene glycol), so as to obtain a resin of the precursor metal with good metal distribution. To obtain the catalyst, each metal is stoichiometrically mixed with carbon Vulcan XC-72 or any other support and heat-treated at high temperatures; e.g., 300–400 °C. This method furnishes robust catalysts with experimental composition close to the nominal one, and our group has employed it for the synthesis of a series of PtSn/C materials [4,23–25]. Nevertheless, the catalytic activity for ethanol electrooxidation is currently under 1.0 A g_{Pt}^{-1}. Hence, proper control of particle morphology and metal distribution must be improved.

Microwave-assisted heating (MW) has gained importance due to its operational simplicity, efficiency, and reduced preparation time [1,20,32]. This method promotes rapid reduction of the metallic precursors and is responsible for the achievement of nanometric particle sizes [33].

In this context, the aim of this work is to carry out a systematic study of PtSn/C nanoparticles and compare the nanoparticles obtained by MW with those prepared by DPP in terms of composition, morphology, and catalytic activity for ethanol electrooxidation.

Table 1
Average particle size (*d*, nm) for the PtSn/C electrocatalysts prepared by different literature methods

Method	Metal load (%)	Composition	*d* (TEM) (nm)	*d* (XRD) (nm)	Reference
BH	20	$Pt_{(25-75)}Sn_{(75-25)}$	2.3	2.2	[11]
	20	$Pt_{75}Sn_{25}$	3.0	–	[18]
AR	20	$Pt_{50}Sn_{50}$	–	2.7	[3]
	20	$Pt_{52}Sn_{48}$	3.0	2.5	[20]
	20	$Pt_{52}Sn_{48}$	–	2.0	[21]
FA	20	$Pt_{51}Sn_{49}$	6.6	3.6	[22]
	20	$Pt_{77}Sn_{33}$	4.5	3.9	[16]
Pechini	40	$Pt_{78}Sn_{22}$	5.0	7.4	[23]
	40	$Pt_{(56-85)}Sn_{(44-15)}$	2.0–10.0	–	[24]
	30	$Pt_{(52-85)}Sn_{(48-15)}$	3.0	–	[25]
	20	$Pt_{75}Sn_{25}$	3.6	–	[26]
	40	$Pt_{72}Sn_{28}$	8.2	6.5	[27]
Polyol	20	$Pt_{70}Sn_{30}$	3.5–8.5	2.8–6.5	[28]
	20	$Pt_{57}Sn_{43}$	–	4.0	[9]
MW/EG	20	$Pt_{35}Sn_{65}$	4.2	3.9	[28]
MW/EG	40	$Pt_{70}Sn_{30}$		4.6	This work
MW/EtOH	40	$Pt_{73}Sn_{27}$	2.8	2.0	This work
MW/PG	40	$Pt_{(66-87)}Sn_{(23-13)}$		3.0–4.8	This work

BH: borohydride reduction; AR: alcohol reduction; FA: formic acid; MW/EG: microwave-assisted ethylene glycol; MW/EtOH: microwave-assisted ethanol; MW/PG: microwave-assisted propylene glycol.

2. Experimental

2.1. Catalysts preparation

Catalysts with nominal composition $Pt_{75}Sn_{25}$/C and 40 wt.% metal loading were prepared by microwave-assisted heating (MW) and thermal decomposition of polymeric precursors (DPP), in order to obtain particles with nanometric dimensions and significant catalytic activity for ethanol electrooxidation. Table 2 depicts the experimental conditions investigated for the MW nanoparticles, in order to optimize nanoparticle size and activity.

Before the synthesis, Carbon Vulcan XC-72 was functionalized in HNO_3 65 wt.% (Merck) under reflux at 80 °C, for 6 h. Next, the carbon was washed, filtered, and dried in an oven at 80 °C. Finally, the powder was heated to 400 °C under N_2 atmosphere, for 4 h. The nanocatalyst prepared by MW was obtained by mixing 1.1 mL 0.077 mol L^{-1} $H_2PtCl_6.6H_2O$ (Aldrich) aqueous solution with 1.4 mL

Table 2
Characterization parameters for the $Pt_{75}Sn_{25}$/C catalyst prepared MW method (1–9) and DPP method (10).

Electrocatalysts							*D* (nm)	
Synthesis	Reducing agent	Stabilizing agent (SA)	Metal: SA molar ratio	Experimental composition[a]	*a* (nm)	Alloy degree (%)	XRD	TEM
1	EtOH	–	–	$Pt_{73}Sn_{27}$	0.3939	5	2.3	2.7
2	EG	–	–	$Pt_{70}Sn_{30}$	0.3942	6	4.6	3.9
3	PG	–	–	$Pt_{66}Sn_{34}$	0.3988	21	3.0	3.8
4	PG	CA	1:1	$Pt_{87}Sn_{13}$	0.3937	4	3.4	–
5	PG	NaAc	1:1	$Pt_{71}Sn_{29}$	0.3979	18	3.9	–
6	PG	NaAc	1:3	$Pt_{70}Sn_{30}$	0.3977	17	4.8	–
7	PG	NaAc	1:5	$Pt_{69}Sn_{31}$	0.3978	18	4.8	2.8
8	PG	NaAc	1:7	$Pt_{87}Sn_{13}$	0.3914	−0.3	2.0	2.5
9	PG	NaAc	1:9	$Pt_{86}Sn_{14}$	0.3925	0.6	2.0	–
10	–	–	–	$Pt_{61}Sn_{39}$	0.3928	2	6.5	8.1

EtOH: ethanol; EG: ethylene glycol; PG: 1,2-propanediol; CA: citric acid; NaAc: sodium acetate.
[a] Assessed by EDX as a mean value among three measurements in different parts of the sample.

0.02 mol L^{-1} $SnCl_2.2H_2O$ (Aldrich) ethanolic solution in 25 mL reducing agent (ethylene glycol, ethanol, or propylene glycol). The mixture was stirred for 5 min in ultrasonic bath, and enough carbon Vulcan XC-72 powder was then added to the mixture, in order to achieve catalysts with 40 wt.% metal load. The mixture was kept under ultrasound stirring for 30 min, until a homogeneous suspension was obtained. This suspension was then placed in a common household microwave oven (Panasonic NN-ST568WRU, 2450 Hz, 800 W) for 60 s. Finally, the suspension was filtered and washed with acetone (Merck), and the solid product was dried in an oven at 120 °C, for 2 h, under N_2 atmosphere. The microwave heating curve for the reducing agent was constructed by measuring the temperature at 10-s intervals, as described elsewhere [34]. The effect of the stabilizing agent, citric acid (CA), and sodium acetate (NaAc) was investigated in propylene glycol medium. The following metal/stabilizing agent molar ratios were investigated: 1:1, 1:3, 1:5, 1:7, and 1:9.

The $Pt_{75}Sn_{25}$/C catalyst was prepared by DPP, by following the description described elsewhere [23–25]. The metallic Pt and Sn resins were prepared separately. Briefly, citric acid (CA) (Merck) was mixed with ethylene glycol (EG) (Merck) at 60–65 °C. The metal precursor (H_2PtCl_6, Aldrich or tin citrate, TC, prepared as described before [31]) was then added to this mixture. A CA/EG/TC molar ratio of 3:10:1 or a CA/EG/Pt molar ratio of 1:4:0.25 was employed. After total dissolution of the precursor salt, the temperature was raised to 90 °C, and the mixture was kept under vigorous stirring for 2–3 h. The DPP catalyst was obtained by mixing the appropriate amount of the Pt or Sn metallic resin with 5.0 mL ethanol. Enough treated carbon Vulcan XC-72 powder was added to the mixture, in order to achieve a catalyst mixture with 40 wt.% metal loading. Finally, the mixture was homogenized in ultrasonic bath and calcined using a temperature program similar to the one described previously [24]. The samples were heated under N_2 – flux (0.05 L min^{-1}) to 250 °C at a rate of 1 °C min^{-1} and were then kept at this temperature for 60 min. After that, the temperature was raised to 350 °C at a rate of 10 °C min^{-1} and maintained at this level for 120 min.

2.2. Physical and chemical characterization

The diffraction patterns were obtained on an X-ray diffractometer (D5005 Siemens) operating with Cu-Kα radiation (λ = 1.5406 Å) generated at 40 kV and 40 mA. The following parameters were kept constant during the analysis: 2θ range = 20°–90°, step = 0.03°, and total analysis time = 1.97 h.

The catalyst phase composition and the position relative to the Kα_1 monochromatic radiation were achieved by fitting the target experimental angular range of interest to the pseudo-Voigt function per crystalline peak with the aid of the Profile Plus Executable refinement program (Siemens AG). The crystallite size values were calculated using the Debye–Scherrer equation [27].

The unit cell parameters were determined by a computer program (U-Fit.exe v1.3-1992) using the least-squares method. The 2θ experimental values and the reflection planes (hkl) were employed for calculation of the unit cell.

Catalyst particle composition was examined by energy dispersive X-ray (EDX) analysis using a Leica microscope Zeiss LEO 440 model SEM coupled to an Oxford 7060 model analyzer.

The morphology of the catalysts was also investigated by Transmission Electron Microscopy (TEM) using a Philips CM120 microscope equipped with LaF_6 filament.

2.3. Electrocatalytic activity

To perform the electrochemical measurements, 2.0 mg catalyst powder were dispersed into a solution (100 μL) consisting of ethanol (95 μL) and Nafion® (5 μL) (5 wt.% in aliphatic alcohols, Aldrich). The mixture was homogenized in ultrasonic bath for 10 min. After homogenization, 20 μL suspension were deposited onto a vitreous carbon electrode (0.2 cm^2) previously polished with alumina (0.3 μm), followed by drying in an oven at 80 °C, for 5 min. The electrochemical measurements were carried out in a conventional three-electrode electrochemical cell (50 mL) using a potentiostat Autolab (PGSTAT-30). A Reversible Hydrogen Electrode (RHE) and a spiralized platinized platinum wire were used as reference and counter electrode, respectively.

The electrochemical characterization of the catalysts was accomplished by cyclic voltammetry (potential range 0.05–1.0 V *vs.* RHE) and chronoamperometry (0.4 V *vs.* RHE for 30 min). The concentrations of the supporting electrolyte (H_2SO_4, Merck) and ethanol (Merck) were kept constant at 0.05 mol L^{-1} and 1.0 mol L^{-1}, respectively.

The electrochemically active area (EAA) of the electrocatalysts was calculated by the CO-stripping technique, which involved oxidation of a monolayer of CO to CO_2, as described elsewhere [35].

All the solutions were prepared with Millipore Milli-Q water® (18.2 MΩ cm at 20 °C). Before accomplishment of the electrochemical measurements, the electrolyte solution was purged with N_2, to expel dissolved oxygen.

2.4. IR spectroscopic measurements

FTIR spectra were measured using 0.05 mol L^{-1} of ethanol solution and 0.05 mol L^{-1} H_2SO_4 as supporting electrolyte. The

electrochemical cell was fitted with a CaF_2 flat window. The FTIR experiments were conducted on a Bruker IFV 66v spectrometer with data acquisition techniques, which allowed us to perform Single Potential Alteration Infrared Reflectance Spectroscopy (SPAIRS). The reflectance spectra were calculated as the ratio $(R - R_0/R_0)$ of a sample (R) and a reference (R_0) spectrum. The spectra were computed from an average of 532 interferograms, and the spectral resolution was set to 8 cm^{-1}. The spectra were recorded in the 1000–3000 cm^{-1} spectral range at 50 mV intervals, between 0.1 and 1.0 V *vs*. RHE during the ethanol oxidation and CO-stripping experiments performed at 1 mV s^{-1}. For the chronoamperometric experiments, the reflectivities were recorded at 1-min intervals for 30 min, at 0.5 V *vs.* RHE.

For the measurements, 5 μL catalyst ink (1 mg catalyst + 99 μL ethanol + 1 μL Nafion®) were deposited onto a gold substrate previously polished with alumina (0.3 μm).

2.5. Fuel cell test

The membrane electrode assemblies (MEAs) were prepared by hot-pressing a pretreated Nafion® 117 membrane placed between an E-TEK cathode (2 mg_{Pt} cm^{-2}) and a homemade anode (2 mg_{Pt} cm^{-2}) at 130 °C for 90 s, under a pressure of 35 kg cm^{-2}. The operating fuel cell performances were determined in a single DEFC with a 5.3 cm^2 geometric surface area of electrodes using a test bench (Eletrocell). The temperature of the fuel cell and the oxygen humidifier were set to 80 and 85 °C, respectively. The ethanol and oxygen pressures were set to 1 and 3 bar, respectively. The ethanol concentration was kept constant at 2 mol L^{-1}. The E (V) *vs*. j (mA cm^{-2}) and P (mW cm^{-2}) *vs*. j (mA cm^{-2}) curves were recorded.

3. Results and discussion

3.1. Effect of reducing and stabilizing agents on the catalysts prepared by MW

The efficiency of reducing agents in terms of nanoparticles stabilization and prevention of metal cluster formation depends on the oxidizing species that is generated during the heating process [17]. Oxidation of small-chain alcohols occurs through interaction between the hydroxyl group(s) present in these molecules and the metallic ions (Pt^{2+}, Sn^{2+}). The latter are subsequently reduced to metal particles and carbonyl and/or carboxyl species are formed. These species adsorb onto the metal particle surface, thereby promoting metal stabilization and preventing their agglomeration as well as the consequent formation of small particles [36].

Table 2 lists the EDX results for the $Pt_{75}Sn_{25}$/C catalysts obtained from the different preparation conditions investigated in the MW synthesis. Changes in the reducing agent (routes 1–3) do not promote significant alterations in the EDX experimental/nominal values, which confirms our previous hypothesis that the reducing agents employed here meet all the requirements for MW heating; e.g., high reduction rate, high capacity for conversion of electromagnetic energy into thermal energy, and suitable temperature profile for the reduction of all the Pt and Sn ions. Propylene glycol (PG) and ethanol give rise to higher catalytic activity, but PG has been selected for further investigation of the effect of the stabilizing agent because it prevents mass loss during MW heating.

The effect of the nature of the stabilizing agent, CA or NaAc, on the catalyst metal loading, routes 4–9, is depicted in Table 2. The EDX data show that the introduction of NaAc improves the reduction of both Pt and Sn to the same extend, resulting in experimental compositions close to the nominal ones. Addition of CA as stabilizing agent leads to an opposite behavior. The beneficial effect of NaAc on the nanoparticle (routes 5–9) can be obtained up to a 1:5 Metal/NaAc molar ratio, but Sn reduction is hindered thereafter. Hence, the 1:5 ratio was considered to be the optimized condition for the synthesis of $Pt_{75}Sn_{25}$/C catalysts by MW in propylene glycol. This result can be understood by taking the complex formed between the stabilizing agent and the metal ions (agent–metal ion pair) into account [37]. Up to the 1:5 ratio, the metal ions are more labile in solution, because the metal-stabilizing agent ionic pair is weak. As the acetate content is raised, the number of ionic pairs also increases, which drastically diminishes the number of free metallic ions in solution (Pt^{2+}, Sn^{2+}). Above the 1:5 ratio, there is significant decrease in the number of Sn and Pt nanoparticles, showing that the stabilizing agent begins to inhibit reduction of the metallic ions. Indeed, incomplete Pt reduction was detected by a qualitative test, which revealed the presence of Pt-ions in propylene glycol solution after the MW treatment.

3.2. Physico-chemical characterization of the nanoparticles

The TEM images and particle size distribution of the $Pt_{75}Sn_{25}$/C materials prepared by the MW or DPP methods are displayed in Fig. 1. MW gives particle size distribution centered between 2.7 and 3.8 nm. Moreover, all the catalysts prepared by MW have nanoparticles homogeneously distributed on the carbon support. Ethanol as reducing agent affords the smallest particle size (2.7 nm). The addition of CA culminates in the formation of Pt clusters, whereas the addition of NaAc avoids variation in particle size and promotes good nanoparticle distribution on the support. Increasing NaAc concentrations, namely 1:7 metal/NaAc ratio, diminishes particle size (2.0 nm). In this case, EDX analysis on isolate nanoparticles reveals that the metallic phase has heterogeneous distribution, with a large amount of Pt particles appearing alone. TEM images of the $Pt_{75}Sn_{25}$/C catalyst prepared by the DPP method evidences that this material consists of nanoparticle clusters with much larger particle sizes (8.14 nm) as compared to the catalyst produced by the optimized MW method (2.87 nm).

Fig. 2 presents the X-ray diffraction pattern of the $Pt_{75}Sn_{25}$/C composition prepared by both investigated methods. The peak at $2\theta = 25°$ is attributed to the (002) crystallographic plane of the carbon support. The peaks detected for all the compositions are characteristic of the crystalline structure of face-centered cubic (fcc) platinum (space group Fm-3m) and refer to the reflection planes (111), (200), (220), (311), and (222). The atomic radius of Sn is larger than the atomic radius of Pt, so the 2θ values shift to the left, indicating alloy formation. The displacements of the 2θ diffraction peaks as compared to pure Pt ($a = 0.39231$ nm) can thus be taken as a measurement of the degree of Sn incorporation into the Pt structure (JCPDS # 00-004-0802). The MW method employing propylene glycol affords a significantly different lattice parameter ($a = 0.3988$ nm, route 3) as compared to the syntheses conducted in ethanol ($a = 0.3939$ nm, route 1) and ethylene glycol ($a = 0.3942$ nm, route 2). The larger shifts in the 2θ diffraction peaks verified for route 3 are in agreement with the EDX data and are typical of Sn incorporation into the Pt structure. This observation is relevant in terms of the modulation of particles by the catalyst, since modification of the reducing medium not only enhances Sn incorporation, but also increases the alloy character of the material.

The effect of the stabilizing agent is shown in Fig. 2C. At lower acetate concentrations; i.e., Metal/NaAc molar ratios up to 1:5, there is a shift in 2θ to lower values, as compared to the structure of pure Pt. This indicates that Sn is incorporated into the Pt fcc structure. However, Pt displacement no longer occurs in the presence of larger acetate amounts (Fig. 2D). The 2θ values shift to values close to that of pure Pt particles, which is evidence of diminished alloy character.

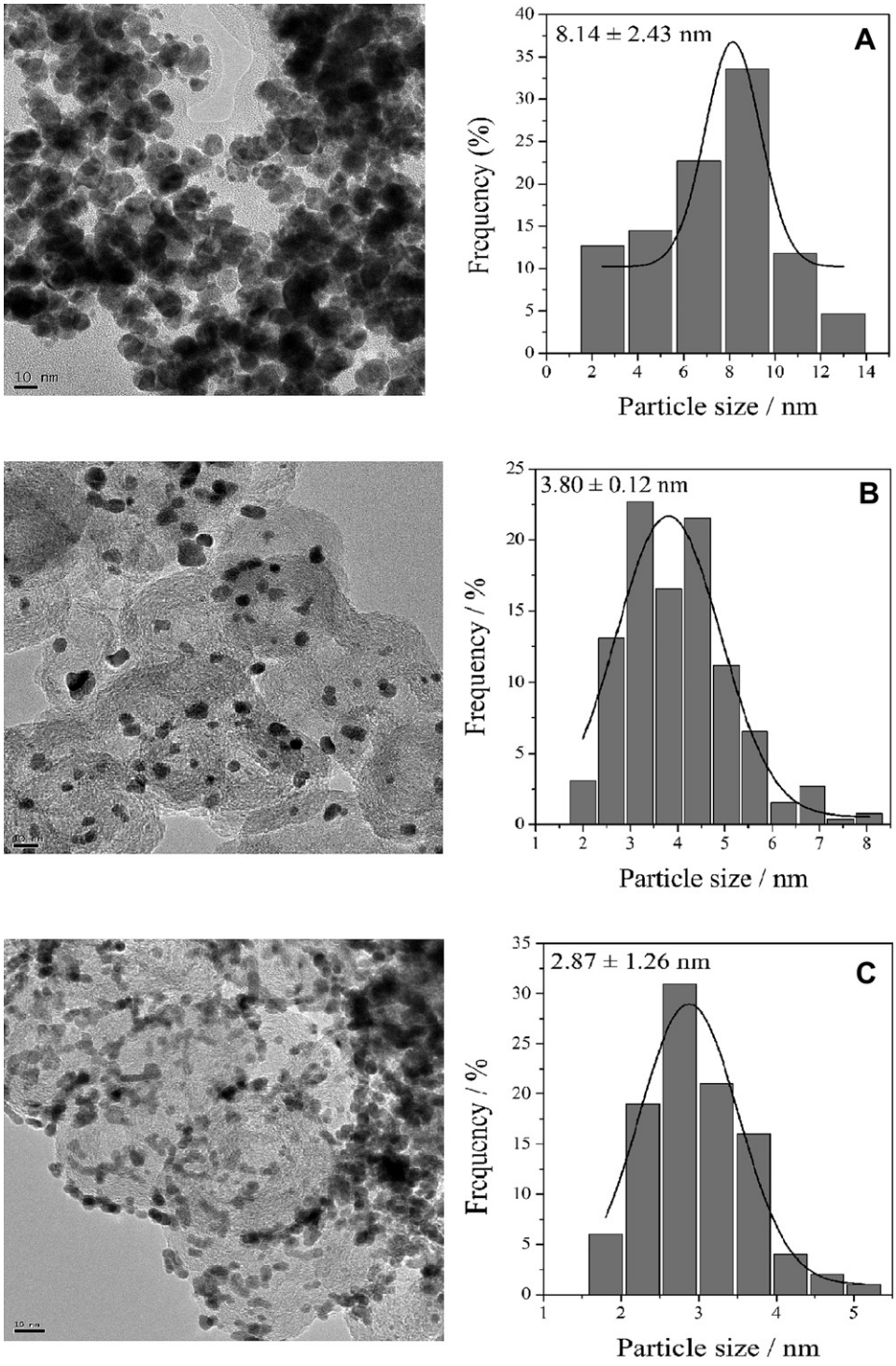

Fig. 1. Representative TEM micrographs of the PtSn/C catalyst prepared by the DPP and MW methods. (A) $Pt_{61}Sn_{39}$/C-DPP; (B) $Pt_{66}Sn_{34}$/C-MW prepared in propylene glycol; and (C) $Pt_{69}Sn_{31}$/C-MW prepared in propylene glycol at Metal/NaAc 1:5 ratio.

PtSn/C nanoparticles prepared by DPP exhibit Pt diffraction peaks with the lattice parameter characteristic of (fcc) Pt (0.3928 nm), which suggests a slight tendency to alloying (Fig. 2A). Besides that, there is phase segregation with formation of Pt_3Sn ($a = 0.40014$ nm), as revealed by the XRD reflection peaks from the cubic structure of Pt_3Sn corresponding to planes (220), (311), and (222) (JCPDS # 01-035-1360).

The alloy degree was determined with the aid of Vegar's law, as described in Ref. [38], and the results are listed in Table 2. The catalyst prepared by DPP is the only one to exhibit phase segregation and to give low alloy degree (2%). The same behavior has also been verified for the catalysts prepared by MW in the presence of ethanol (5%), ethylene glycol (6.1%), and citric acid (4.5%). PG and NaAc up to a 1:5 ratio furnish nanocatalysts with expressive alloy degree; i.e., 17–21%. Increasing the PG/NaAc ratio to values higher than 1:5 results in a sharp drop of the alloy degree (0.6% for a 1:7 ratio), and alloy formation is not detected at all when PG and NaAc are added at a 1:9 ratio (−0.3%).

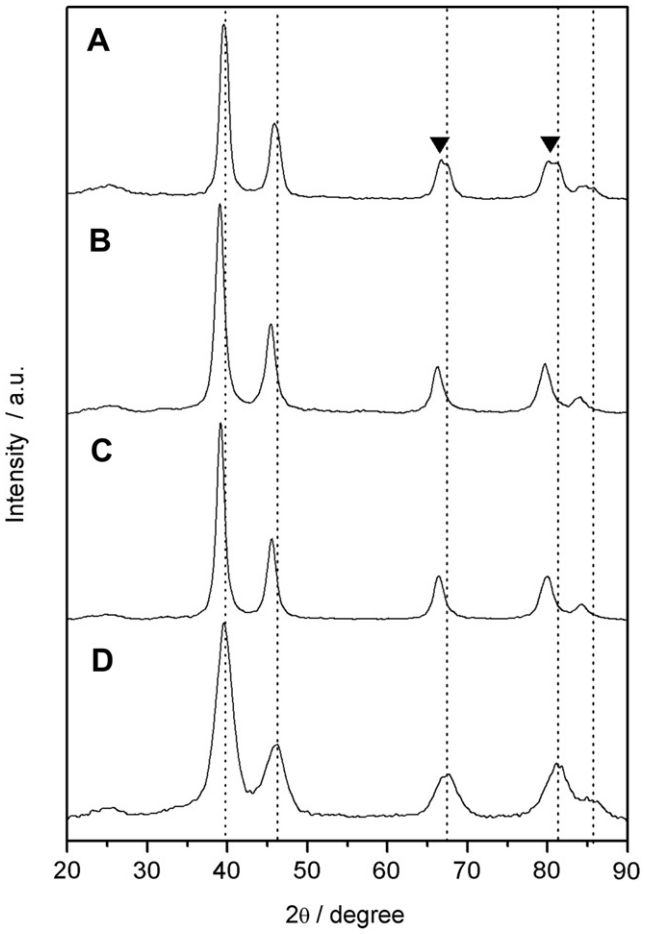

Fig. 2. XRD patterns of the PtSn/C catalysts prepared by the DPP and MW methods. (A) $Pt_{61}Sn_{39}$/C-DPP; (B) $Pt_{66}Sn_{34}$/C-MW prepared in propylene glycol; (C) $Pt_{69}Sn_{31}$/C-MW prepared in propylene glycol at Metal/NaAc 1:5 ratio; and (D) $Pt_{87}Sn_{13}$/C-MW prepared in propylene glycol at Metal/NaAc 1:7 ratio. (▼) Pt_3Sn phase.

The Pt (311) reflection plane was used for calculation of the average crystallite size according to the Scherrer equation [27]. The average crystallite size of PtSn/C-MW might be related to the efficiency of the reducing agents in oxidizing the Pt and Sn ions and forming the stabilizing species that prevents the formation of metal particle clusters. On the basis of the data presented in Table 2, it can be inferred that ethanol undergoes faster oxidation, with consequent acetic acid generation. The latter quickly adsorbs onto the metal nuclei, giving rise to smaller nanoparticles (2.7 nm). In this work, ethylene glycol and propylene glycol afforded larger nanocatalyst particle size, around 4.0 nm, because stabilization of the metallic cores probably takes place more slowly as compared with ethanol.

In the presence of sodium acetate, the crystallite size ranges from 3.0 nm to 4.8 nm for Metal/NaAC ratios lying in the 1:0–1:5 range, but it decreases abruptly thereafter. This behavior contrasts with the one reported in the literature for pure Pt nanoparticles [17,39] and can be understood in terms of the differences in the bimetallic nanoparticles reduction rate.

The average crystallite size of PtSn/C-MW (4.8 nm, in the optimized conditions) is smaller than that of PtSn/C-DPP (6.5 nm). This agrees with the data obtained by TEM analysis, which also revealed smaller nanoparticles for PtSn/C-MW (2.8 nm) as compared to PtSn/C-DPP (8.1 nm). The formation of smaller nanoparticles by MW can be attributed to the fast heating taking place during the MW method. This promotes rapid nucleation of the nanoparticles and avoiding nanoparticles growing.

3.3. Electrochemical characterization

Fig. 3 brings representative cyclic voltammograms of the different catalysts in a 0.05 mol L^{-1} H_2SO_4 solution. PtSn/C-MW catalysts have high voltammetric charge as compared to PtSn/C-DPP. This behavior agrees with the particle size characterization and indicates that MW promotes the formation of a higher amount of Pt catalytic sites. The cyclic voltammograms obtained for all the catalysts synthesized by MW using different reducing agents or sodium acetate as stabilizing agent display similar voltammetric behavior. None of the synthetic conditions furnished a catalyst with a well-defined hydrogen adsorption/ desorption region.

The electrochemically active area of the nanocatalyst (EAA) was calculated by CO-stripping voltammetric experiments. The default value for the oxidation of a CO monolayer ($Q_{CO}o$) on a smooth polycrystalline platinum electrode is 420 μC cm^{-2} [35]. Thus, the EAA was calculated by normalizing the electrochemical charge relative to $Q_{CO}o$. Table 3 summarizes the EAA values found for the $Pt_{75}Sn_{25}$/C catalysts.

Regarding the catalysts prepared by MW, the use of ethanol as reducing agent allows for the attainment of catalysts with EAA of 70.2 m^2 g_{Pt}^{-1}. This is twice the value of those obtained in the presence of ethylene glycol and propylene glycol, with EAA values of 36.5 m^2 g_{Pt}^{-1} and 35.5 m^2 g_{Pt}^{-1}, respectively. It can be inferred from Table 3 that there is no correlation between the presence of a stabilizing agent and the EAA. MW yields catalysts with EAA at least four to seven times larger (35–70 m^2 g_{Pt}^{-1}) than the values obtained for the catalysts prepared by DPP (8.0 m^2 g_{Pt}^{-1}). Once the EDX results showed that there is no significant difference between the catalysts synthesized by MW and DPP in terms of chemical composition, the marked changes in EAA can be ascribed to diminished particle size and better distribution of the Pt sites over the carbon support in the case of MW.

Another parameter that enables comparison between the different nanoparticles synthesized herein is the determination of the Pt chemical specific surface area (CSA, m^2 g_{Pt}^{-1}) following equation (1), as described in Ref. [40]. The CSA considers the determination of all the Pt surface available for the oxidation reaction, assuming that all particles are spherical.

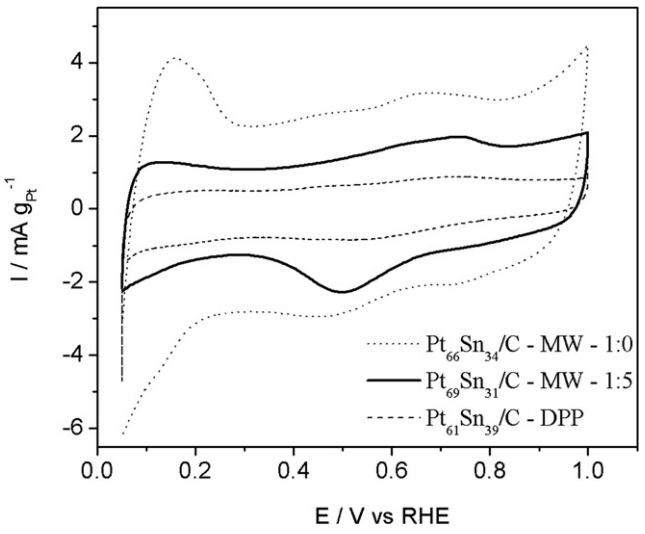

Fig. 3. Representative cyclic voltammograms of the PtSn/C electrocatalysts in 0.05 mol L^{-1} H_2SO_4 supporting electrolyte at 10 mV s^{-1}.

Table 3
Catalytic performance[a] for ethanol and CO oxidation as a function of synthesis method. MW method (1–9) and DPP method (10).

Synthesis	E_{onset} (V)	Activity (A g_{Pt}^{-1})	j (mA cm^{-2})	E_{CO} (V)	EAA (m^2 g_{Pt}^{-1})	CSA (m^2 g_{Pt}^{-1})	[b]EAA/CSA (%)
1	0.22	9.8	5.7	0.37	70.22	121.90	58
2	0.21	6.5	3.6	0.36	36.50	60.95	60
3	0.16	7.0	3.7	0.28	35.51	93.46	38
4	0.20	2.1	1.5	0.22	30.49	82.46	37
5	0.21	5.1	2.9	0.31	52.32	71.89	73
6	0.14	9.1	5.1	0.42	39.80	58.41	68
7	0.18	12.2	6.7	0.20	35.00	58.41	60
8	0.16	11.0	7.7	0.24	51.80	140.19	37
9	0.17	11.1	7.6	0.41	43.30	140.19	31
10	0.30	0.21	0.10	0.43	8.0	35.05	23

[a] Values measured at fixed potential (0.4 V *vs.* RHE).
[b] Pt available (%).

$$\text{CSA} = \frac{6 \times 10^3}{pd}\left(\text{m}^2\ \text{g}_{\text{Pt}}^{-1}\right) \quad (1)$$

where ρ is the Pt density of (21.4 g cm^{-3}) and d (nm) is the diameter of the Pt particles in the catalyst, as calculated from XRD results (see Table 2). As the CSA values depend on crystallite size, a catalyst with smaller crystallite size has larger CSA, as seen in Table 3. The CSA is larger than EAA because not all the Pt surface is electrocatalytically active for a reaction process. Thus, the EAA/CSA ratio can furnish the percentage of Pt available for ethanol oxidation in each catalyst and can be determined by using equation (2) [40].

$$\text{Pt available}\ (\%) = \frac{\text{EAA}}{\text{CSA}} \times 100 \quad (2)$$

Table 3 contains the results of Pt available and shows that all the catalysts prepared by MW have the largest values as compared to PtSn/C-DPP (only 23%). Route 5 (Metal/NaAc ratio 1:5) has the highest Pt available (73%), as well as the catalysts prepared in ethanol and ethylene glycol.

The onset potential for the CO oxidation reaction confirms that the PtSn/C-MW catalysts display lower overpotential for CO oxidation (0.20 *vs.* RHE) as compared to PtSn/C-DPP (0.43 *vs.* RHE). Among the MW catalysts, the 1:5 Metal/NaAc ratio affords the lowest overpotential for CO oxidation.

3.4. Ethanol electrooxidation

Fig. 4 corresponds to representative cyclic voltammograms for ethanol oxidation obtained for the PtSn/C catalysts. Current values in the hydrogen adsorption/desorption region are not achieved for any of the compositions, due to ethanol adsorption onto the Pt sites. The current achieved for ethanol oxidation in the case of the DPP catalyst is much smaller as compared to the MW catalysts. At potentials lower than 0.4 V *vs.* RHE, there are no significant differences in the current generated in the presence of ethanol for any of the MW catalysts. The main changes appear at higher potentials, where two small peaks located at 0.45 and 0.8 V *vs.* RHE are detected for the catalyst synthesized in propylene glycol medium. Addition of the stabilizing agent enhances the ethanol oxidation current, with consequent disappearance of the multiple peaks. This unusual electrochemical behavior of the anode material could be interpreted as a continuous renewal of the catalytic sites associated with a constant removal of any poisoning species from the surface over the whole potential domain. The changes in the electrocatalytic activity might be due to structural effects, as observed previously [41,42]. The current increases up to a 1:3 Metal/NaAc ratio and remains steady thereafter.

The potential for the onset of ethanol oxidation (E_{onset}) was determined from the intersection between the two linear portions of the voltammogram. Table 3 summarizes the obtained results. E_{onset} determination is a good parameter for selection of the best catalyst for ethanol oxidation. Indeed, the best material is the one with the lowest ethanol oxidation potential. Analysis of Table 3 shows that all the PtSn catalysts present low E_{onset} − values as compared to the pure Pt catalyst (0.45 *vs.* RHE). The beneficial effect of Sn introduction into the Pt catalyst can be notice and makes Pt–Sn catalysts the most promising materials for ethanol oxidation [4,11–13]. To improve such catalytic activity, there are two approaches. One is the introduction of a third metal into the metallic alloy, as discussed frequently in the literature [9,12,19,20,23,27,30]. This is because the third metal improves the Sn effect and enhances the activity of the alloy towards ethanol oxidation. The second approach involves introduction of morphological changes into the catalyst by means of a different synthesis method, as reported here. In this work, the average potential for the onset of ethanol oxidation (E_{onset}) is shown to be lower for PtSn/C-MW (0.18 V *vs.* RHE in optimized conditions) as compared to PtSn/C-DPP (0.30 V *vs.* RHE).

The catalytic mass activity was evaluated by chronoamperometry in a 1.0 mol L^{-1} ethanol solution by applying a potential of 0.4 V *vs.* RHE for 30 min. Fig. 5 illustrates some representative chronoamperometric curves, and Table 3 contains the current activity values. All the investigated catalysts display similar current decay pattern.

Inicitally, there is an abrupt decay in current probably due to catalyst poisoning by organic species chemisorbed onto the Pt sites.

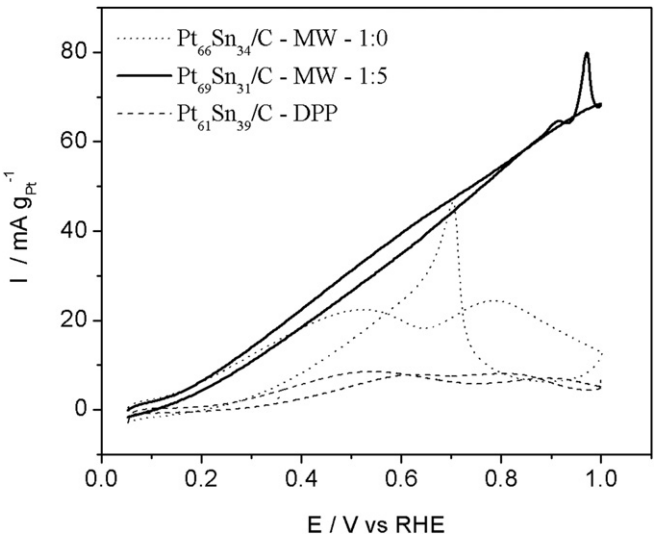

Fig. 4. Representative cyclic voltammograms of the PtSn/C electrocatalysts in 1.0 mol L^{-1} ethanol + 0.05 mol L^{-1} H_2SO_4 supporting electrolyte at 10 mV s^{-1}.

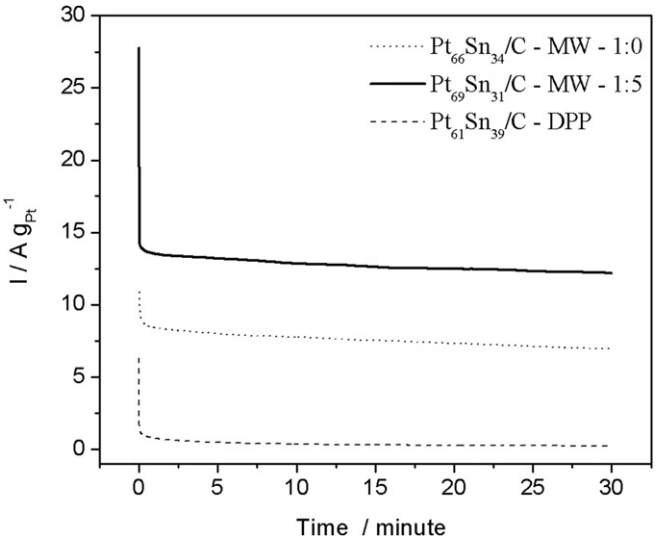

Fig. 5. Current *vs.* time plots for the electrooxidation of 1.0 mol L^{-1} ethanol in 0.05 mol L^{-1} at 0.4 V *vs.* RHE for the prepared PtSn/C catalysts.

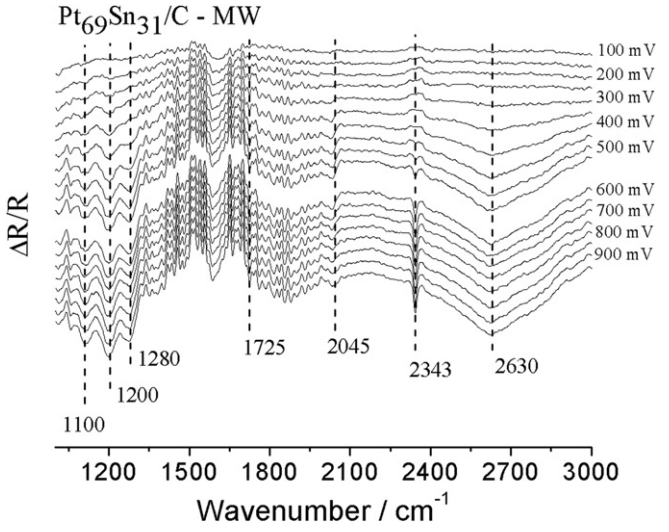

Fig. 6. SPAIRS spectra of the species coming from ethanol (0.05 mol L^{-1}) adsorption and oxidation in 0.05 mol L^{-1} H_2SO_4 on a $Pt_{69}Sn_{31}$/C-MW catalyst at different potentials.

Thereafter, an almost constant current value is achieved on $Pt_{69}Sn_{31}$/C-MW. Although the $Pt_{66}Sn_{34}$/C composition prepared under the same condition (MW) has less current than the previous one, their behavior is similar for a long period. The stability of current densities may be explained by a good crystallization of the particles prepared by the MW method. Conversely, the particles issued from the DPP method have low current likely due to high diameter particles with few active sites on the electrode surface [23].

In the case of the MW route carried out in the absence of the stabilizing agent, the highest catalytic activity is obtained for the catalysts prepared in ethanol medium. Chronoamperometric curves depend greatly on the stabilizing agent. For instance, the use of CA (route 4) leads to poor activity, as compared to the material prepared in NaAc medium. The Sn content in the mixture material composition and the presence at the surface or in the core may play a key role in the bifunctional mechanism towards the ethanol reaction on the Pt-based anode catalyst [27,43]. As result, samples #8 and #9 have lower Sn contents but exhibit high activities. This denotes that structural effects due to a better particle distribution may also play an important role in the activity. Again, evidence that the PtSn/C-MW prepared at a Metal/NaAC ratio 1:5 is able to achieve higher electrocatalytic activity (12.0 A g_{Pt}^{-1}) at 30 min as compared to PtSn/C-DPP (0.21 A g_{Pt}^{-1}). This suggests that the MW method affords more active particles, in agreement with their smaller size and better distribution over the carbon support.

Fig. 6 shows the representative SPAIRS spectra obtained for ethanol oxidation on $Pt_{69}Sn_{31}$/C-MW (route 5).

There is an intense band at 1640 cm^{-1}, related to interfacial water, as well as a strong feature at 1200 cm^{-1}, due to an increase in the concentration of HSO_4^- ions in the thin layer of the solution between the electrode and the IR window. This anion is mainly formed via reaction of SO_4^{2-} with the H^+ produced during the oxidation reaction [24,44].

The band at 1100 cm^{-1} is attributed to acetaldehyde formation [45]. Acetic acid formation is evidenced by the bands at 1280 cm^{-1}, which corresponds to C–O stretching, while the –OH deformation from the –COOH group appears at 1390 cm^{-1}. The presence of this molecule is also evidenced by the simultaneous appearance of the large band centered at 2630 cm^{-1}. The band at 1725 cm^{-1}, assigned to the carbonyl group C=O stretching, confirms the presence of acetaldehyde and acetic acid. Acetaldehyde and acetic acid formation starts at 0.30 and 0.35 V *vs.* RHE, respectively. The acetaldehyde peak intensity is more evident for the $Pt_{61}Sn_{39}$/C-DPP catalyst as compared to $Pt_{69}Sn_{31}$/C-MW, although there is no change in the potential where this band appears. Little acetic acid is formed at the DPP catalyst; i.e., the band at 1280 cm^{-1} is not observed, and a very weak band is obtained at 2630 cm^{-1}.

CO/CO_2 formation is also related to the investigated synthetic route. The MW catalysts exhibit the band characteristic of carbon monoxide linearly adsorbed (CO_L) (2035 cm^{-1}) onto the Pt site at 0.3 V *vs.* RHE. Above 0.4 V *vs.* RHE, CO_L undergoes oxidation to CO_2, which is verified by the presence of a band located at 2343 cm^{-1}. On the other hand, the DPP catalyst does not present the CO_L band, and CO_2 formation starts at 0.6 V *vs.* RHE. These results confirm our previous finding about the electrochemical behavior of catalysts prepared by different routes.

The chronoamperometric/IR investigation was carried out by applying 0.5 V *vs.* RHE for 30 min at a fixed ethanol concentration (0.05 mol L^{-1}). Acetaldehyde is the only product in the case of the $Pt_{61}Sn_{39}$/C-DPP catalyst; whereas four oxidation products are observed for $Pt_{69}Sn_{31}$/C-MW, namely acetaldehyde, acetic acid, CO_L, and CO_2. These results corroborate the SPAIRS data and reveal that the MW catalysts are stronger when it comes to improving the ethanol electrooxidation rate ($n_e^- > 2$), while the DPP route furnishes a milder configuration ($n_e^- = 2$).

Fig. 7 depicts the CO_L and CO_2 band intensities as a function of the potential during the CO-stripping/IR experiments. The CO molecule has been as probe, since it allows for comparison of material efficiency. Compared to $Pt_{61}Sn_{39}$/C-DPP, $Pt_{69}Sn_{31}$/C-MW adsorbs CO in greater amounts. This behavior agrees with the percentage of Pt available sites previously calculated for each catalyst in the present work. Indeed the catalyst synthesized by MW has been shown to have larger Pt utilization sites, 60%, against 23% for the catalyst prepared by DPP. It is also worth mentioning that though CO_2 formation begins at the same potential (0.35 V *vs.* RHE) for both catalysts, CO oxidation on $Pt_{69}Sn_{31}$/C-MW starts at lower potential values as compared with $Pt_{61}Sn_{39}$/C-DPP. The IR results are in broad agreement with the physical and electrochemical characterization of the compositions and confirm that the catalysts prepared by MW are more active for ethanol and CO oxidation.

The outstanding catalytic activity obtained for PtSn/C-MW makes it very promising for application in DEFC as compared, for

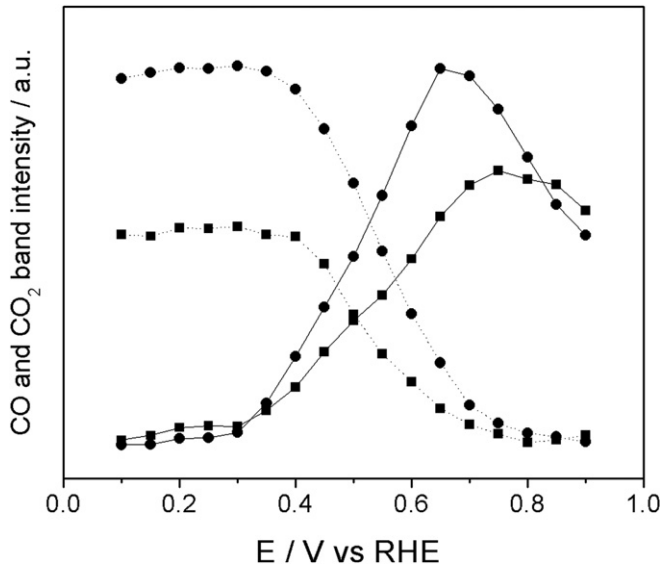

Fig. 7. Normalized intensities of the CO_L (solid line) and CO_2 (dashed line) bands in the CO-stripping/IR experiment. (●) $Pt_{69}Sn_{31}$/C-MW and (■) $Pt_{61}Sn_{39}$/C-DPP.

instance, to other PtSn catalysts prepared by different routes, such as the catalyst produced by Spinacé et al. [20] via the formic acid reduction method. In the latter case, the resulting Pt:Sn (50:50) catalyst displayed catalytic activity of 6 A g_{Pt}^{-1}, measured at similar conditions employed here, namely 0.5 V *vs.* RHE. In another investigation, Neto et al. [31] reported activity of 9 A g_{Pt}^{-1} for the Pt:Sn (50:50) catalyst prepared by the alcohol reduction method.

Fig. 8 contains the cell performance at 80 °C for some representative PtSn/C catalysts prepared here. The open circuit potentials are 0.74 V and 0.72 V for the MW (Metal/NaAc, 1:5) and DPP routes, respectively, indicating good similarity between these methods and other catalysts frequently found in the literature [4,16,24,25]. However, there is a pronounced difference in the power density intensities: the MW catalysts display higher values as compared to the DPP catalyst, namely 37 mW cm^{-2} against 24 mW cm^{-2}. The fuel cell performance confirms the electrochemical and physical characterization, indicating that smaller

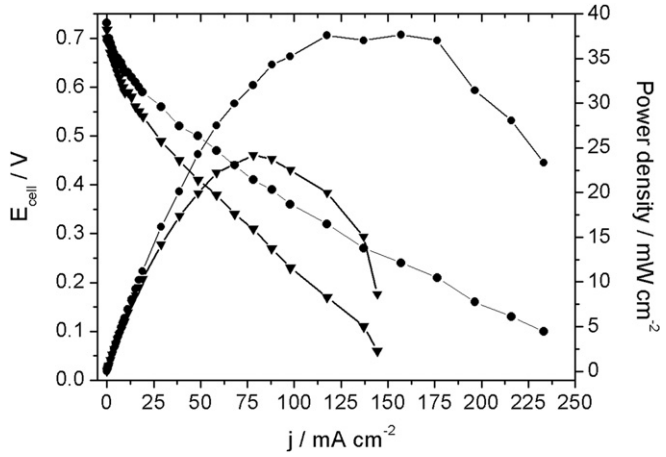

Fig. 8. Cell voltage (V) and power density (mW cm^{-2}) *vs.* current density (mA cm^{-2}) on DEFC with 5.29 cm^2 area at 80 °C using the PtSn/C anodes prepared by DPP and MW (2 mg cm^{-2} catalyst loading, 60 wt.% catalyst on carbon). $P(O_2)$ = 3 bar; P(EtOH) = 1 bar; [EtOH] = 2.0 mol L^{-1}; Nafion® 117 membrane. (●) $Pt_{69}Sn_{31}$/C-MW and (■) $Pt_{61}Sn_{39}$/C-DPP.

particle size and better homogeneous distribution on the carbon platform determine higher efficiency for ethanol oxidation in DEFC. This result makes the MW synthesis very promising. In this context, ternary compositions are currently under investigation in our group, with a view to achieving higher power densities.

4. Conclusions

We have demonstrated that the microwave-assisted heating process can be effectively used for the preparation of PtSn/C catalysts with high current densities. This heating method is simple and requires short preparation time, which is advantageous as compared to the DPP method and other routes proposed in the literature. Our optimization studies have shown that particle size and catalytic activity are strongly dependent on the employed reducing and stabilizing agents. The results have clearly evidenced that the use of propylene glycol and sodium acetate as reducing and stabilizing agents, respectively, produces materials with average particle size ranging from 2.0 to 5.0 nm, with catalytic activity exceeding 12 A g_{Pt}^{-1} and low overpotential for ethanol oxidation. The 1:5 Metal/NaAC ratio produces the most active catalyst; i.e., small nanoparticle size, better particle distribution on the carbon support, and higher catalytic activity towards ethanol electrooxidation. The electrochemical characterizations are in agreement with the physical characterizations. There is pronounced alloy formation in the case of the PtSn/C catalysts prepared by MW, where particles of smaller sizes are homogeneously distributed on the carbon support. This culminates in larger EAA, which accounts for the excellent electrocatalytic activity. The use of CO as probe molecule showed that PtSn/C-MW is capable of oxidizing it to CO_2 at lower potentials. This demonstrates electrode material synthesized by a simple route, is a promising anode catalyst for DEFC applications. The fuel cell performance of the catalysts prepared by the MW method (37 mW cm^{-2}) confirms its higher activity as compared to the catalysts synthesized by DPP (24 mW cm^{-2}).

Acknowledgements

Financial support from FAPESP and CAPES is gratefully acknowledged. T.S. Almeida acknowledges the Ph.D fellowship under the contract number FAPESP 2009/15034-2. The authors thank the LNLS Synchrotron Laboratory for the use of the TEM microscope.

References

[1] X. Li, W.X. Chen, J. Zhao, W. Xing, Z.D. Xu, Carbon 43 (2005) 2168–2174.
[2] F. Hu, C. Chen, Z. Wang, G. Wei, P.K. Shen, Electrochim. Acta 52 (2006) 1087–1091.
[3] A.O. Neto, R.W.R. Verjulio-Silva, M. Linardi, E.V. Spinace, Int. J. Electrochem. Sci. 4 (2009) 954–961.
[4] D.M. dos Anjos, F. Hahn, J.M. Léger, K.B. Kokoh, G. Tremiliosi-Filho, J. Braz. Chem. Soc. 19 (2008) 795–802.
[5] W.J. Zhou, Z.H. Zhou, S.Q. Song, W.Z. Li, G.Q. Sun, P. Tsiakaras, Q. Xin, Appl. Catal. B 46 (2003) 273–285.
[6] F.H.B. Lima, E.R. Gonzalez, Electrochim. Acta 53 (2008) 2963–2971.
[7] F. Maillard, E. Peyrelade, Y. Soldo-Olivier, M. Chatenet, E. Chainet, R. Faure, Electrochim. Acta 52 (2007) 1958–1967.
[8] Z.L. Liu, X.Y. Ling, X.D. Su, J.Y. Lee, L.M. Gan, J. Power Sources 149 (2005) 1–7.
[9] A. Bonesi, G. Garaventa, W.E. Triaca, A.M. Castro Luna, Int. J. Hydrogen Energy 33 (2008) 3499–3501.
[10] T.C. Deivaraj, W.X. Chen, J.Y. Lee, J. Mater. Chem. 13 (2003) 2555–2560.
[11] D.-H. Lim, D.-H. Choi, W.-D. Lee, H.-I. Lee, Appl. Catal. B 89 (2009) 484–493.
[12] E.V. Spinace, L.A. Farias, M. Linardi, A.O. Neto, Mater. Lett. 62 (2008) 2099–2102.
[13] F.J. Nores-Pondal, I.M.J. Vilella, H. Troiani, M. Granada, S.R. de Miguel, O.A. Scelza, H.R. Corti, Int. J. Hydrogen Energy 34 (2009) 8193–8203.
[14] Z.L. Liu, X.Y. Ling, X.D. Su, J.Y. Lee, J. Phys. Chem. B 108 (2004) 8234–8240.
[15] F.J. Vidal-Iglesias, A. Al-Akl, D.J. Watson, G.A. Attard, Electrochem. Commun. 8 (2006) 1147–1150.

[16] F. Colmati, E. Antolini, E.R. Gonzalez, Appl. Catal. B 73 (2007) 106–115.
[17] J. Zhao, W. Chen, Y. Zheng, X. Li, Z. Xu, J. Mater. Sci. 41 (2006) 5514–5518.
[18] D.R.M. Godoi, J. Perez, H.M. Villullas, J. Power Sources 195 (2010) 3394–3401.
[19] A. Oliveira Neto, R.R. Dias, M.M. Tusi, M. Linardi, E.V. Spinace, J. Power Sources 166 (2007) 87–91.
[20] E.V. Spinace, R.R. Dias, M. Brandalise, M. Linardi, A. Oliveira Neto, Ionics 16 (2010) 91–95.
[21] E.V. Spinace, L.A.I. do Vale, R.R. Dias, A. Oliveira Neto, M. Linardi, in: E.M. Gaigneaux, et al. (Eds.), Scientific Bases for the Preparation of Heterogeneous Catalysts, Proceedings of the 9th International Symposium (2006), pp. 617–624.
[22] E. Antolini, F. Colmati, E.R. Gonzalez, Electrochem. Commun. 9 (2007) 398–404.
[23] J. Ribeiro, D.M. dos Anjos, J.M. Léger, F. Hahn, P. Olivi, A.R. de Andrade, G. Tremiliosi-Filho, K.B. Kokoh, J. Appl. Electrochem. 38 (2008) 653–662.
[24] F.L.S. Purgato, P. Olivi, J.M. Leger, A.R. de Andrade, G. Tremiliosi-Filho, E.R. Gonzalez, C. Lamy, K.B. Kokoh, J. Electroanal. Chem. 628 (2009) 81–89.
[25] F.C. Simoes, D.M. dos Anjos, F. Vigier, J.M. Leger, F. Hahn, C. Coutanceau, E.R. Gonzalez, G. Tremiliosi-Filho, A.R. de Andrade, P. Olivi, K.B. Kokoh, J. Power Sources 167 (2007) 1–10.
[26] R.F.B. De Souza, L.S. Parreira, D.C. Rascio, J.C.M. Silva, E. Teixeira-Neto, M.L. Calegaro, E.V. Spinace, A.O. Neto, M.C. Santos, J. Power Sources 195 (2010) 1589–1593.
[27] T.S. Almeida, K.B. Kokoh, A.R. De Andrade, Int. J. Hydrogen Energy 36 (2011) 3803–3810.
[28] Z.L. Liu, B. Guo, L. Hong, T.H. Lim, Electrochem. Commun. 8 (2006) 83–90.
[29] N. Toshima, T. Yonezawa, New J. Chem. 22 (1998) 1179–1201.
[30] E. Antolini, F. Colmati, E.R. Gonzalez, J. Power Sources 193 (2009) 555–561.
[31] M.P. Pechini, Patent number 3.330.697, USA, 1967.
[32] F. Kadirgan, S. Beyhan, T. Atilan, Int. J. Hydrogen Energy 34 (2009) 4312–4320.
[33] M. Tsuji, M. Hashimoto, Y. Nishizawa, M. Kubokawa, T. Tsuji, Chem. Eur. J. 11 (2005) 440–452.
[34] W.X. Tu, H.F. Liu, J. Math. Chem. 10 (2000) 2207–2211.
[35] D.M. Dos Anjos, K.B. Kokoh, J.M. Léger, A.R. De Andrade, P. Olivi, G. Tremiliosi-Filho, J. Appl. Electrochem. 36 (2006) 1391–1397.
[36] C. Bock, C. Paquet, M. Couillard, G.A. Botton, B.R. MacDougall, J. Am. Chem. Soc. 126 (2004) 8028–8037.
[37] S. Ozkar, R.G. Finke, J. Am. Chem. Soc. 124 (2002) 5796–5810.
[38] E. Antolini, Mater. Chem. Phys. 78 (2003) 563–573.
[39] J.W. Guo, T.S. Zhao, J. Prabhuram, C.W. Wong, Electrochim. Acta 50 (2005) 1973–1983.
[40] S. Yin, P.K. Shen, S. Song, S.P. Jiang, Electrochim. Acta 54 (2009) 6954–6958.
[41] J.-M. Leger, B. Beden, C. Lamy, S. Bilmes, J. Electroanal. Chem. Interfacial Electrochem. 170 (1984) 305–317.
[42] A. Kowal, M. Li, M. Shao, K. Sasaki, M.B. Vukmirovic, J. Zhang, N.S. Marinkovic, P. Liu, A.I. Frenkel, R.R. Adzic, Nat. Mater. 8 (2009) 325–330.
[43] E. Antolini, J.R.C. Salgado, E.R. Gonzalez, J. Electroanal. Chem. 580 (2005) 145–154.
[44] E.A. Batista, G.R.P. Malpass, A.J. Motheo, T. Iwasita, J. Electroanal. Chem. 571 (2004) 273–282.
[45] S. Garcia-Rodriguez, S. Rojas, M.A. Pena, J.L.G. Fierro, S. Baranton, J.M. Leger, Appl. Catal. B 106 (2011) 520–528.